Journal of Membrane Science & Research

journal homepage: www.msrjournal.com

Research Paper

# Polytetrafluoroethylene Membrane Design for Ammonia Transfer and Future Sensor Integration in Water

Maulana Fakih Latief [1,*], Benfano Soewito [1], Maria Susan Anggreainy [1], Suryadiputra Liawatimena [1]

*Computer Science Department, BINUS Graduate Program, Doctor of Computer Science, Bina Nusantara University, Jakarta 11480, Indonesia*

## Article info

Received 2026-05-19
Revised 2026-06-12
Accepted 2026-06-12
Available online 2026-06-12

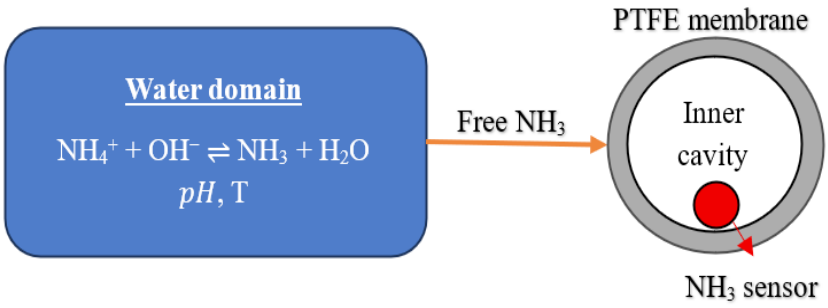
## Keywords

Ammonia sensing
Spherical PTFE membrane
$NH_3$ transfer
COMSOL modeling
Wetting safety

## Highlights

- A spherical PTFE membrane was modeled for ammonia transfer in water.
- Free $NH_3$ was defined from the water-side ammonium-ammonia equilibrium.
- Membrane geometry strongly affected ammonia accumulation in the cavity.
- Wetting safety was evaluated using pore size and hydrostatic pressure.
- A design envelope was proposed for future cost-effective $NH_3$ sensors.

## Graphical abstract




## Abstract

Ammonia sensing in water requires a membrane interface that enables $NH_3$ transfer while limiting liquid intrusion into the sensor cavity. This study develops a physics-based COMSOL framework to evaluate a spherical polytetrafluoroethylene (PTFE) membrane for $NH_3$ transfer and future gas sensor integration in water. The framework explicitly considers the water-side $NH_4^+/NH_3$ equilibrium, where $NH_4^+$ is used to estimate available free $NH_3$ but is not modeled as the transported species through the membrane. The model evaluates membrane thickness, inner diameter, pore size, active pore-area fraction, pH, temperature, $NH_4^+$ concentration, and placement depth. Results show that transfer-favorable configurations may reduce wetting resistance. Although the 22 µm pore baseline produced 6.2425 × $10^{-4}$ mol/m³ $NH_3$ at 100 s, its wetting-safety factor was only 1.5214. The recommended design used 1.0 mm thickness, 22 mm inner diameter, 10 µm pores, and 0.75 active pore-area fraction, balancing $NH_3$ transfer, wetting resistance, structural feasibility, and sensor-cavity compatibility.

© 2026 FIMTEC & MPRL. All rights reserved.

### 1. Introduction

Membrane-based gas transfer has attracted increasing attention in water-related applications because it enables controlled mass transfer across a selective barrier while maintaining separation between gas and liquid phases. Among membrane materials, polytetrafluoroethylene (PTFE) is widely regarded as promising because of its hydrophobicity, chemical inertness, structural stability, and suitability for membrane-contactor and membrane-distillation applications [1–3]. These properties make PTFE relevant for membrane-assisted gas sensing in water, where the membrane is expected to allow gas transport while limiting direct liquid intrusion into the sensor chamber.

Ammonia-related water sensing requires careful definition of the transferred species. In water, ammonia exists in equilibrium between ammonium ions and free ammonia, $NH_4^+ <=> NH_3 + H^+$. Recent studies on ammonia recovery using membrane distillation, membrane contactors, and PTFE-based membranes have shown that $NH_3$ transfer is strongly affected by pH, temperature, membrane characteristics, and operating conditions [4–6]. In the present study, the relevant transfer pathway is the movement of neutral $NH_3$ from the water side into the inner cavity where a future $NH_3$ gas sensor may be placed, rather than the direct transport of $NH_3$.

* Corresponding author: maulana.latief@binus.ac.id (M. F. Latief)

DOI: 10.22079/jmsr.2026.2087860.1753

Gas-transfer performance is governed not only by membrane material but also by membrane geometry and water-side conditions. For a spherical PTFE membrane, the key geometrical parameters include inner diameter, membrane thickness, pore size, and active pore-area fraction, whereas the main water-side factors include placement depth, pH, temperature, and $NH_4^+$ concentration. Studies on membrane-based nitrogen recovery similarly indicate that material properties, module configuration, and operating conditions are critical in nitrogen separation systems [7]. These factors affect transfer response, free $NH_3$ availability, and resistance to water intrusion. Therefore, pore size, wettability, and antiwetting behavior must be considered when assessing membrane feasibility under liquid exposure [8,9]. Accordingly, membrane selection should be evaluated within a physical design envelope rather than based on transfer magnitude alone.

Although gas-permeable membranes have been studied for gas transfer and ammonia recovery, the design of a spherical PTFE membrane for future $NH_3$ gas sensor integration in water remains insufficiently addressed [10,11]. Previous studies have given limited attention to how spherical geometry, $NH_4^+/NH_3$ equilibrium, hydrostatic pressure, pore-related wetting resistance, and wetting-safety constraints jointly define membrane feasibility. This gap is important because a sensor-oriented membrane must enable sufficient $NH_3$ transfer into the inner cavity while preventing water intrusion.

To address this need, this study develops a COMSOL-based physics-informed framework for evaluating a spherical PTFE membrane for $NH_3$ transfer in water. Compared with flat-sheet and hollow-fiber geometries commonly used in separation and recovery-oriented membrane modules, the spherical PTFE configuration is more aligned with the sensing-oriented design requirement because it provides a protected inner cavity where $NH_3$ transfer, gas accumulation, and future sensor placement can be evaluated together. The main objective is to establish a physics-based design envelope that links membrane geometrical characteristics, active pore-area distribution, water-side ammonia conditions, and wetting-safety constraints for future $NH_3$ gas sensor integration. Therefore, the novelty of this study lies in formulating a spherical PTFE membrane design framework for sensor-oriented $NH_3$ transfer in water. Based on this objective, the study is guided by the following research questions:

RQ1: How do the geometrical characteristics of a spherical PTFE membrane, including inner diameter, membrane thickness, pore size, and active pore-area fraction, influence $NH_3$ transfer from water into the inner cavity?

RQ2: How do water-side conditions, including placement depth, $pH$, temperature, and $NH_4^+$ concentration, influence free $NH_3$ availability, $NH_3$ transfer, and wetting safety in a spherical PTFE membrane system?

RQ3: What design envelope of a spherical PTFE membrane is suitable for future $NH_3$ gas sensor integration, considering membrane geometry, water-side $NH_4^+$ concentration, free $NH_3$ availability, and wetting-safety constraints?

## 2. Theoretical Background

### 2.1. $NH_3$ Transfer in PTFE Membrane–Water Systems

Membrane contactors provide an interface for gas–liquid mass transfer without direct mixing of the two phases. In such systems, transfer behavior is governed by the concentration gradient across the membrane and by the resistance offered by both the membrane structure and the surrounding medium. PTFE is commonly considered suitable for water-related membrane applications because of its hydrophobicity, chemical inertness, and structural stability [1,2]. These properties are important for membrane-assisted sensing in water, where the membrane is expected to allow gas transport while limiting direct liquid intrusion into the sensing cavity.

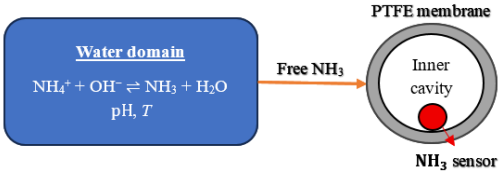



**Fig. 1.** Conceptual framework of membrane-assisted $NH_3$ transfer through a spherical PTFE membrane for future gas-sensor integration.

As illustrated in Fig. 1, the spherical PTFE membrane is interpreted as a gas-permeable porous barrier that supports the transfer of neutral ammonia gas, $NH_3$, from the water side into the inner cavity. The membrane is not assumed to transport ammonium ions, $NH_4^+$, directly. Instead, the relevant transfer species is the free ammonia fraction, $NH_3$, generated from the water-side ammonium/ammonia equilibrium. Therefore, the membrane-transfer process is modeled as a concentration-driven transport problem for an $NH_3$-equivalent species through an effective porous PTFE domain. This interpretation is consistent with the intended future configuration, in which an $NH_3$ gas sensor may be placed inside the spherical cavity while the surrounding water contains ammonium-related species.

### 2.2. $NH_4^+/NH_3$ Equilibrium in Water

Ammonia in water exists in an acid–base equilibrium between ammonium ion and free ammonia:

$$NH_4^+ \rightleftharpoons NH_3 + H^+ \tag{1}$$

In this equilibrium, $NH_4^+$ is the ionized ammonium form, while $NH_3$ is the neutral free ammonia form. Since PTFE is hydrophobic and gas-permeable, the transfer pathway considered in this study is associated with $NH_3$, not direct transport of $NH_4^+$. The availability of free $NH_3$ is primarily controlled by pH and temperature. Recent ammonia-related membrane studies have also shown that pH strongly influences ammonia partitioning and membrane-based mass transfer [5,6].

The equilibrium relationship is expressed using the Henderson–Hasselbalch equation:

$$\mathrm{pH} = \mathrm{p}K_a + \log\left(\frac{[NH_3]}{[NH_4^+]}\right) \tag{2}$$

Rearranging gives:

$$\frac{[NH_3]}{[NH_4^+]} = 10^{(\mathrm{pH}-\mathrm{p}K_a)} \tag{3}$$

Accordingly, when the water-side ammonium concentration is represented by $[NH_4^+]$, the estimated free ammonia concentration can be written as:

$$[NH_3] = [NH_4^+] \times 10^{(\mathrm{pH}-\mathrm{p}K_a)} \tag{4}$$

In the simulation framework, this relationship is implemented as:

$$C_{NH_3,water} = C_{NH_4,water} \times 10^{(\mathrm{pH}-\mathrm{p}K_a)} \tag{5}$$

where $C_{NH_4,water}$ is the water-side ammonium concentration and $C_{NH_3,water}$ is the estimated free ammonia concentration available for membrane transfer. This formulation connects the planned $NH_4^+$-based water-side sensing condition with the $NH_3$ gas-transfer pathway through the PTFE membrane. Importantly, $C_{NH_4,water}$ is not treated as the species transported through PTFE; it is used only to estimate the free $NH_3$ concentration available at the water side. This concentration-based equilibrium formulation is used as a design-level approximation for dilute freshwater conditions. Activity coefficients are not explicitly included because the present study focuses on controlled early-stage membrane design for freshwater sensing conditions.

The value of $\mathrm{p}K_a$ is temperature dependent and is estimated as:

$$\mathrm{p}K_a = 0.09018 + \frac{2729.92}{T} \tag{6}$$

where $T$ is the water temperature in Kelvin. This relation shows that increasing pH shifts the equilibrium toward free $NH_3$, while lower pH favors

$NH_4^+$. Temperature also affects the equilibrium by changing $pK_a$. Consequently, even when the water-side ammonium concentration is constant, the amount of $NH_3$ available for membrane transfer may change substantially with pH and temperature.

### 2.3. Effective Porous Transport Through the PTFE Membrane

The spherical PTFE membrane system is represented as a concentration-driven mass-transfer problem. The governing transport equation for species movement in free and porous domains is expressed as:

$$\frac{\partial c}{\partial t} + \nabla \cdot J = R \tag{7}$$

where $c$ is the $NH_3$-equivalent concentration, $J$ is the mass flux, and $R$ is the source or reaction term. In the present study, no chemical reaction is modeled inside the PTFE membrane domain, so $R = 0$ within the membrane. The source concentration on the water side is determined by the $NH_4^+ / NH_3$ equilibrium.

Diffusive transport is represented using Fick's law:

$$J = -D_{\text{eff}} \nabla c \tag{8}$$

where $D_{\text{eff}}$ is the effective diffusivity. For porous transport through the PTFE membrane, the effective membrane diffusivity is expressed as:

$$D_{\text{mem,eff}} = \frac{\varepsilon_{\text{eff}}}{\tau} D \tag{9}$$

where $D$ is the molecular diffusivity, $\tau$ is tortuosity, and $\varepsilon_{\text{eff}}$ is the effective active porosity. In this design-level model, the effective active porosity is expressed as:

$$\varepsilon_{\text{eff}} = \varepsilon_{\text{PTFE}} f_{\text{active}} f_{\text{opening}} \tag{10}$$

where $\varepsilon_{\text{PTFE}}$ is the nominal PTFE porosity, $f_{\text{active}}$ is the effective active pore-area fraction, and $f_{\text{opening}}$ is the normalized pore-opening factor. Pore connectivity is therefore not resolved explicitly and is treated as part of the effective porous-medium representation. The pore-opening factor is approximated as:

$$f_{\text{opening}} = \left( \frac{d_p}{d_{p,\max}} \right)^2 \tag{11}$$

This expression is based on the area dependence of pore opening on pore diameter and is used as a design-level approximation rather than a microscopic pore-resolved model. Accordingly, the membrane is treated as an effective porous medium whose properties can be mapped to controllable prototype variables, including membrane thickness, pore size, and active membrane area. This design-level transport interpretation is consistent with recent ammonia membrane-modeling and CFD-based membrane-contactor studies [13,14].

### 2.4. From Ammonia Recovery to Ammonia Sensing

Ammonia recovery refers to the process of transferring ammonia from a liquid stream to another phase or capture medium so that ammonia can be removed, concentrated, or reused. In membrane-based ammonia recovery, ammonium-containing water is commonly conditioned so that a fraction of dissolved ammonium shifts into neutral free ammonia, $NH_3$. The neutral $NH_3$ can then transfer across a membrane interface, while the liquid phase remains separated from the receiving side. Previous studies have shown that ammonia recovery and transfer are influenced by pH, temperature, membrane characteristics, capture solution, and system configuration [4–6,10–12]. Therefore, ammonia recovery studies provide a relevant theoretical basis for understanding $NH_4^+ / NH_3$ equilibrium, $NH_3$ partitioning, membrane-based transfer, and operating-condition effects.

The transition from ammonia recovery to ammonia sensing lies in the design objective. In recovery-oriented systems, membrane transfer is generally directed toward capturing, removing, or concentrating ammonia from liquid streams [4,7,10–12]. In sensing-oriented systems, the objective is not ammonia capture as a product, but controlled $NH_3$ transfer into a protected sensor cavity where the gas can be exposed to a detection element. Recent $NH_3$ gas sensor studies have demonstrated low-level ammonia detection using material-based and electrochemical sensing approaches [20,21]. In the present study, recovery-derived membrane-transfer principles are redirected toward ammonia sensing by evaluating a spherical PTFE membrane that enables measurable $NH_3$ accumulation in an inner cavity for future gas sensor exposure while limiting direct liquid intrusion. Thus, ammonia recovery literature provides the physicochemical and membrane-transfer foundation, whereas the present design envelope is formulated for membrane-assisted ammonia sensing in water.

### 2.5. Wetting Constraint Under Water Immersion

Because the membrane is intended to operate in water, design feasibility is not determined only by $NH_3$ transfer response. The PTFE membrane must also resist water intrusion into the pores and inner cavity. Therefore, wetting safety is evaluated using the relationship between hydrostatic pressure and liquid-entry pressure. Previous studies on PTFE membranes show that wetting resistance is closely related to pore size, surface chemistry, surface roughness, and contact angle [8,15].

The hydrostatic pressure at the membrane depth is calculated as:

$$P_{\text{hydro}} = \rho g z \tag{12}$$

where $\rho$ is water density, $g$ is gravitational acceleration, and $z$ is the membrane placement depth.

The liquid-entry pressure of the hydrophobic PTFE membrane is estimated using:

$$\text{LEP}_{\text{PTFE}} = \frac{-4B\gamma \cos\theta}{d_p} \tag{13}$$

where $B$ is a pore-geometry factor, $\gamma$ is the surface tension of water, $\theta$ is the water contact angle on PTFE, and $d_p$ is the pore diameter. In this study, $B = 1$ is used as a first-order cylindrical pore approximation.

The wetting-safety factor is defined as:

$$SF_{\text{wetting}} = \frac{\text{LEP}}{P_{\text{hydro}}} \tag{14}$$

A value of $SF_{\text{wetting}} > 1$ indicates that the estimated liquid-entry pressure is higher than the hydrostatic pressure, while $SF_{\text{wetting}} < 1$ indicates a higher risk of water intrusion. For design-envelope interpretation, a more conservative threshold is applied:

$$SF_{\text{wetting}} \geq 1.5 \tag{15}$$

This condition ensures that membrane selection is not based only on maximum $NH_3$ transfer response but also on physical feasibility under water immersion.

### 2.6. Structural Feasibility of Membrane Thickness

In addition to diffusive performance, membrane thickness must also satisfy a lower-bound structural feasibility criterion. A thinner membrane may reduce diffusion resistance and increase $NH_3$ transfer, but an excessively thin spherical membrane may become physically less feasible under external pressure. Therefore, membrane thickness is evaluated not only as a transport-path parameter but also as a structural design variable.

For a thin spherical shell under external pressure, the critical shell pressure is approximated as:

$$P_{\text{cr}} = \frac{2E}{\sqrt{3(1-\nu^2)}} \left( \frac{t}{R} \right)^2 \tag{16}$$

where $E$ is Young's modulus, $\nu$ is Poisson's ratio, $t$ is membrane thickness, and $R$ is the characteristic shell radius. The Young's modulus used in this first-order structural screening refers to the PTFE material value adopted for design-level feasibility evaluation and does not explicitly account for stiffness reduction induced by membrane porosity. Therefore, the resulting structural safety factor should be interpreted as a lower-bound feasibility indicator rather than a final mechanical durability prediction for porous PTFE. In the present framework, the applied external load is represented by the effective external pressure:

$$\Delta P_{ext} = P_{hydro} + P_{ext} \tag{17}$$

where $P_{hydro}$ is the hydrostatic pressure and $P_{ext}$ is the additional external pressure term used in the model.

The structural safety factor is then defined as:

$$SF_{struct} = \frac{P_{cr}}{\Delta P_{ext}} \tag{18}$$

For conservative design interpretation, the structural criterion is applied as:

$$SF_{struct} \geq 1.5 \tag{19}$$

From this threshold, the minimum thickness required to satisfy the lower-bound structural condition can be estimated as:

$$t_{min,struct} = R\sqrt{\frac{SF_{struct,target}\,\Delta P_{ext}\sqrt{3\left(1-\nu^2\right)}}{2E}} \tag{20}$$

This criterion is used in this study as a first-order lower-bound structural feasibility check. The thin-shell relation in equation (17) serves as an analytical structural screening criterion within the proposed design framework, ensuring that membrane thickness is evaluated not only from diffusive performance but also from first-order structural feasibility under external pressure. This structural screening is not intended to represent long-term durability, creep, fatigue, or aging of PTFE, but to support the construction of a physically meaningful design envelope.

### *2.7. Design-Level Interpretation*

The proposed framework should be interpreted as a physics-informed design-level model rather than a microscopic pore-resolved simulation. The model uses established physical and chemical relations, including $NH_4^+ / NH_3$ equilibrium, Fickian diffusion, hydrostatic pressure, liquid-entry pressure, and lower-bound shell feasibility, while representing pore morphology through effective parameters. This interpretation is appropriate because the objective of the study is to define a feasible design envelope before prototype development and future $NH_3$ gas sensor integration.

Accordingly, the final membrane design should not be selected solely by maximizing transfer response. A thinner membrane, larger pore size, or higher active pore-area fraction may increase $NH_3$ accumulation in the inner cavity, but these trends must be evaluated against wetting resistance, hydrostatic pressure, lower-bound structural feasibility, and practical design requirements for sensor integration. The suitable design is therefore defined as a configuration that provides sufficient $NH_3$ transfer while remaining within the physical safety constraints required for operation in water.

## 3. Related Works

Membrane contactors and related membrane systems have been widely recognized as effective interfaces for gas–liquid mass transfer because they provide a large interfacial area while maintaining separation between gas and liquid phases. In ammonia-related applications, recent studies have shown that membrane distillation and membrane contactor systems can support ammonia removal by promoting the transfer of volatile $NH_3$ across a membrane interface [4]. Broader work on nitrogen recovery also indicates that recent developments have focused on improved membrane materials, module configurations, and process-oriented optimization strategies [7]. These studies indicate that membrane-based transfer systems are already well established in separation and recovery research. However, most studies still focus on conventional membrane configurations, such as hollow-fiber, capillary, tubular, or flat-sheet systems, rather than the design logic of a spherical PTFE membrane immersed in water as a cavity-based transfer structure for future gas sensor integration.

In ammonia-related membrane applications, gas-permeable membranes have been investigated for ammonia recovery under different operating conditions and system configurations. Soto-Herranz et al. showed that capture solution and temperature affect ammonia recovery in suspended gas-permeable membrane systems [10]. In a related study, different tubular gas-permeable membrane configurations produced different ammonia trapping performances, confirming that system arrangement strongly influences recovery effectiveness [11]. In addition, recent ammonia-transport analysis in direct contact membrane distillation has emphasized the coupled behavior of ammonia and water transport during selective ammonia recovery [12]. These studies are important because they show that gas-permeable membranes can support ammonia transfer across a liquid–membrane interface. However, they remain centered on ammonia recovery from manure or wastewater in conventional membrane systems, not on sensor-oriented $NH_3$ transfer from water into an inner cavity through a spherical PTFE membrane.

From the simulation perspective, recent work has demonstrated that physics-based numerical modeling is a credible approach for membrane-transfer analysis. Hu et al. developed a modeling and performance-optimization framework for ammonia recovery via direct contact membrane distillation [13]. Bozonc et al. developed and validated a 3D-CFD model of a hollow-fiber membrane contactor for $CO_2$ absorption, showing that detailed numerical modeling can represent coupled transport behavior in membrane-contactor systems [14]. These studies support the use of numerical simulation as a valid design tool for membrane systems. However, recent simulation studies remain centered on conventional membrane modules and have not established a threshold-based design envelope for spherical PTFE membranes intended to transfer $NH_3$ into an inner cavity for future gas sensor integration.

Recent studies have further shown that membrane transfer performance is strongly influenced by structural and wetting-related characteristics. In PTFE membrane systems, wettability and wetting resistance remain critical issues under demanding feed or immersion conditions [8]. Liquid-entry pressure and antiwetting behavior are strongly affected by pore structure, surface chemistry, surface roughness, contact angle, surface modification, and pore-size control [15–19]. These findings reinforce the importance of evaluating membrane structure not only from transfer performance, but also from resistance to liquid intrusion. However, these studies remain focused mainly on conventional membrane systems and do not address how a spherical PTFE membrane can be designed to balance gas transfer, cavity accumulation, and liquid-entry resistance.

Another important issue in ammonia-related membrane systems is the chemical form of ammonia in water. Ammonia exists in equilibrium between ammonium ion, $NH_4^+$, and free ammonia, $NH_3$, where pH and temperature strongly affect the available free $NH_3$ fraction. This distinction is critical for membrane-assisted sensing because PTFE is not expected to transport $NH_4^+$ ions directly. Instead, the relevant membrane-transfer species is neutral $NH_3$, which can diffuse through the gas-permeable membrane and accumulate in the sensor cavity. Therefore, membrane design for future $NH_3$ gas sensor integration requires not only structural and material considerations, but also explicit consideration of water-side $NH_4^+$ concentration, pH, temperature, and the resulting free $NH_3$ availability.

Recent $NH_3$ gas sensor studies have also demonstrated that low-level ammonia detection is technically feasible. For example, recent material-based and electrochemical $NH_3$ sensor studies reported ppm to sub-ppm detection capability at room temperature [20,21]. These sensor studies support the relevance of designing an inner cavity where $NH_3$ can accumulate for future sensing. However, they do not address the membrane-side design problem required to transfer $NH_3$ from water into a protected sensor cavity.

To clarify the position of the present study within recent literature, Table 1 summarizes the main focus, contribution, and remaining gap of the most relevant prior works and compares them with the present study.

**Table 1**
Summary of Recent Related Works and Research Position.

| Ref. | Main focus | System/object studied | Main variables emphasized | Main contribution | Limitation / research gap relevant to this study |
|---|---|---|---|---|---|
| [4] | Ammonia recovery and removal using hydrophobic membranes | Hydrophobic membrane distillation and membrane contactor systems | Ammonia recovery, membrane process, operating conditions | Summarized recent developments in ammonia recovery and removal using hydrophobic membrane systems | Review focus; does not provide a spherical PTFE design envelope for sensor-oriented $NH_3$ transfer |
| [7] | Membrane technologies for nitrogen recovery | Membrane-based nitrogen recovery systems | Membrane materials, module design, process optimization | Showed that membrane materials and module configurations are important in nitrogen recovery | Broad review; does not address spherical PTFE membrane design for $NH_3$ sensing |
| [8] | PTFE membrane wetting and wettability | Capillary PTFE membranes for membrane distillation | Wettability, wetting resistance, feed conditions | Confirmed that wetting resistance is critical for PTFE membrane performance | Focused on capillary PTFE membranes, not spherical immersed membranes with an inner cavity |
| [10] | Ammonia recovery under different operating conditions | Suspended gas-permeable membrane systems | Capture solution, temperature | Showed that capture solution and temperature affect ammonia recovery | Focused on recovery performance, not sensor-oriented $NH_3$ transfer into a cavity |
| [11] | Ammonia trapping under different configurations | Tubular gas-permeable membrane systems | System configuration, membrane arrangement | Demonstrated that tubular configuration affects ammonia trapping performance | Focused on tubular recovery systems, not spherical PTFE cavity-based sensing design |
| [12] | Ammonia and water transport | Direct contact membrane distillation | Ammonia transport, water transport, selective recovery | Explained coupled ammonia and water transport behavior in selective ammonia recovery | Does not address spherical PTFE geometry or $NH_3$ accumulation in an inner sensor cavity |
| [13] | Modeling and optimization of ammonia recovery | Direct contact membrane distillation | Transport modeling, operating conditions, performance optimization | Demonstrated modeling-based evaluation of ammonia recovery performance | Does not address spherical PTFE membrane geometry or inner-cavity $NH_3$ accumulation |
| [14] | 3D-CFD modeling of membrane contactors | Hollow-fiber membrane contactor for $CO_2$ absorption | 3D transport behavior, module configuration, flow arrangement | Validated CFD-based modeling as a credible framework for membrane-contactor analysis | Focused on hollow-fiber industrial contactors rather than spherical PTFE membranes for $NH_3$ transfer |
| [15] | Liquid-entry pressure characterization | Gas/liquid phase-separation membranes | Liquid-entry pressure, membrane wetting, pressure condition | Provided insight into liquid-entry pressure as a feasibility parameter for gas/liquid membranes | Does not examine $NH_3$ transfer or spherical PTFE sensor-cavity design |
| [16] | Antiwetting hydrophobic surfaces | Hydrophobic membranes for membrane distillation | Surface chemistry, roughness, contact angle, antiwetting behavior | Reviewed strategies for improving antiwetting performance | Does not provide a specific spherical membrane design envelope |
| [17] | Superhydro-phobic PTFE membrane performance | Modified PTFE membrane for membrane distillation | Antiwetting, antifouling, PTFE surface modification | Demonstrated improved antiwetting and antifouling performance in PTFE membranes | Focused on membrane distillation, not $NH_3$ sensing through a spherical cavity |
| [18] | PTFE membrane scaling resistance | CNT-modified PTFE membrane for membrane distillation | Scaling resistance, surface modification, wetting behavior | Demonstrated that PTFE membrane surface modification can improve scaling resistance and reduce wetting-related deterioration | Focused on membrane distillation and scaling control, not spherical PTFE membranes for $NH_3$ sensor-cavity integration |
| [19] | Pore-size-tunable superhydro-phobic membrane | Superhydro-phobic membrane for membrane distillation | Pore size, surface structure, water flux, wetting resistance | Demonstrated that pore-size tuning can improve membrane performance while maintaining superhydrophobic behavior | Focused on high-flux membrane distillation, not $NH_3$ transfer into a spherical sensor cavity |
| [20] | Low-level $NH_3$ gas sensing | Material-based $NH_3$ gas sensor | Response/recovery, detection limit, low-concentration $NH_3$ | Demonstrated fast response/recovery and sub-ppm $NH_3$ sensing capability | Sensor-focused study; does not address water-side membrane transfer |
| [21] | Electrochemical $NH_3$ sensing | Electrochemical ammonia sensor | Room-temperature sensing, detection range, response time | Demonstrated electrochemical $NH_3$ detection over a ppm-level range | Sensor-focused study; does not address PTFE membrane design or water immersion |
| This study | Physics-based design-envelope analysis of $NH_3$ transfer | Spherical PTFE membrane immersed in water with an inner cavity | Inner diameter, membrane thickness, pore size, active pore-area fraction, $NH_4^+/NH_3$ equilibrium, pH, temperature, placement depth, and wetting-safety factor | Proposes a COMSOL-based framework linking membrane geometry, $NH_4^+/NH_3$ equilibrium, $NH_3$ transfer, liquid-entry pressure, wetting safety, and future gas sensor integration | — |

As summarized in Table 1, prior studies have established the importance of membrane material properties, operating conditions, ammonia recovery configurations, wetting resistance, gas sensing, and physics-based modeling in membrane transfer systems. However, the specific case of a spherical PTFE membrane immersed in water has not been systematically addressed in terms of $NH_3$ transfer into an inner cavity for future gas sensor integration. In particular, previous studies have not combined spherical membrane geometry, active pore-area fraction, water-side $NH_4^+/NH_3$ equilibrium, placement-depth-related wetting safety, and design-envelope analysis within a single COMSOL-based framework. This gap motivates the present study, which develops a physics-informed design framework for selecting feasible spherical PTFE membrane characteristics before future $NH_3$ gas sensor integration.

## 4. METHODOLOGY

### *4.1. Research Procedure*

This study was conducted through a staged physics-informed design procedure to evaluate a spherical PTFE membrane for $NH_3$ transfer in water and to define a feasible design envelope for future gas sensor integration. The overall procedure began with the identification of relevant design variables and water-side conditions, followed by the definition of the $NH_4^+/NH_3$ equilibrium as the basis for estimating the free $NH_3$ concentration available for transfer. These inputs were then implemented in a COMSOL-based spherical membrane model to simulate $NH_3$ transfer from the surrounding water, through the PTFE membrane, and into the inner cavity.

After the baseline model was established, parametric simulations were conducted to evaluate the effects of the main geometrical characteristics, namely inner diameter, membrane thickness, pore size, and active pore-area fraction. These geometrical parameters were evaluated together with the main water-side conditions, namely placement depth, pH, temperature, and $NH_4^+$ concentration. The resulting transfer and feasibility metrics were then interpreted together to define a physically feasible design envelope rather than a single maximum-response configuration. The research workflow is summarized conceptually in Fig. 2.

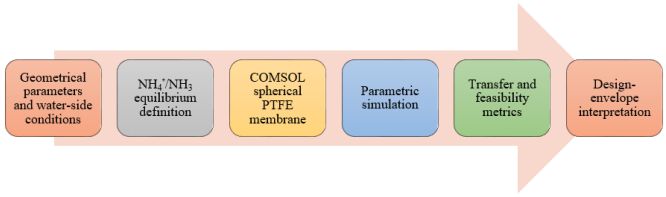



**Fig. 2.** Physics-informed research workflow for spherical PTFE membrane design and design-envelope evaluation.

This staged procedure allows the study to connect physical and chemical inputs, numerical transport behavior, and engineering-design interpretation within a single analysis framework.

### *4.2. COMSOL-Based Modeling Setup*

The simulation model was developed in COMSOL Multiphysics as a three-domain system consisting of the surrounding water domain, the porous PTFE membrane domain, and the inner cavity. The spherical PTFE membrane was treated as the main design object, while the inner cavity represented the intended space for future $NH_3$ gas sensor placement. The water domain provided the ammonia-related source condition, the membrane domain represented the gas-permeable barrier, and the cavity domain represented the enclosed region where $NH_3$ accumulation was evaluated.

In this model, the membrane was not assumed to transport $NH_4^+$ directly. Instead, the transferable species was represented as free $NH_3$ estimated from the water-side $NH_4^+$ concentration, pH, and temperature. The spherical membrane was modeled as an effective porous medium rather than as a pore-resolved microscopic structure. This choice was made because the purpose of the study was to define a design-level envelope for future prototype development, not to reconstruct the detailed spatial arrangement of individual pores. This type of numerical modeling approach is consistent with recent membrane-modeling studies that use simulation to evaluate coupled transport behavior and membrane-system performance [13,14].

At the water–membrane interface, the free $NH_3$ concentration estimated from the $NH_4^+ / NH_3$ equilibrium was prescribed as the boundary concentration driving diffusive $NH_3$ transfer through the PTFE membrane. The water phase and $NH_4^+$ ions were not modeled as transported species through the membrane. Following the governing transport relation in equation (8) and the diffusive flux definition in equation (9), the coupled-domain formulation was defined to preserve diffusive flux continuity between the PTFE membrane and the inner cavity. Since no reaction term was imposed inside the PTFE membrane or cavity domains, $NH_3$ accumulation in the cavity was governed by concentration-driven diffusive transfer across the coupled domains.

The main geometrical characteristics considered in the model were inner diameter, membrane thickness, pore size, and active pore-area fraction. The water-side input parameters were placement depth, pH, temperature, and $NH_4^+$ concentration. The inner diameter determines the cavity size available for $NH_3$ accumulation and future sensor placement. Membrane thickness determines the diffusion path length through the PTFE wall. Pore size affects both the effective transfer opening and the liquid-entry pressure of the membrane. Active pore-area fraction represents the fraction of membrane surface that actively contributes to $NH_3$ transfer.

A baseline configuration was then defined to provide a consistent reference for subsequent parametric analysis. The baseline conditions used in the simulation are summarized in Table 2.

**Table 2**
Baseline Parameters Used in the COMSOL Model.

| Parameter | Symbol | Baseline value | Role in the model |
|---|---|---|---|
| Inner radius | $r_{in}$ | 9 mm | Defines cavity size |
| Membrane thickness | $t_{mem}$ | 1.0 mm | Defines diffusion path length |
| Inner diameter | $D_i$ | 18 mm | Defines sensor cavity dimension |
| Pore size | $d_p$ | 22 µm | Governs transfer opening and liquid-entry pressure |
| Active pore-area fraction | $f_{active}$ | 1.0 | Represents active transfer area |
| Placement depth | $z$ | 0.3 m | Determines hydrostatic pressure |
| pH | pH | 8.5 | Governs free $NH_3$ availability |
| Temperature | $T$ | 298.15 K | Governs equilibrium condition |
| Ammonium concentration | $C_{NH4,water}$ | 1 mol/m³ | Represents water-side ammonia source condition |

The material properties of PTFE were implemented consistently in the model to support both transport analysis and lower-bound structural checking. In addition to transfer-related parameters, the model also included a first-order shell-stability criterion to prevent membrane thickness from being interpreted only as a diffusive parameter.

### *4.3. Output Metrics*

The membrane configurations were evaluated using both transfer-response and feasibility metrics. The primary transfer-response metric was the average $NH_3$ concentration in the inner cavity at a selected observation time. In this study, the cavity concentration at 100 s was used as the main comparative response indicator because it provides a consistent basis for comparing both geometrical and water-side parameter variations.

The second output group was related to wetting feasibility. For this purpose, the model evaluated the hydrostatic pressure associated with the selected placement depth, the liquid-entry pressure of the PTFE membrane, and the wetting-safety factor. These outputs were used to determine whether a membrane configuration remained resistant to water intrusion under the intended immersion condition.

The third output group was related to the lower-bound structural feasibility of membrane thickness. A first-order shell-stability check was used to estimate the critical shell pressure, the structural safety factor, and the corresponding minimum thickness required to remain above the selected structural threshold. This allowed membrane thickness to be interpreted not only from transfer response, but also from physical feasibility.

Accordingly, the main output metrics in this study were:

1. average $NH_3$ concentration in the inner cavity at 100 s;
2. hydrostatic pressure;
3. liquid-entry pressure;
4. wetting-safety factor;
5. critical shell pressure;
6. structural safety factor; and
7. estimated minimum structural thickness.

These output metrics were selected so that the membrane could be evaluated from both performance and feasibility perspectives rather than from transfer magnitude alone.

### *4.4. Design-Envelope and Model Scope*

The final stage of the methodology interpreted the simulation outputs within a design-envelope framework. In this study, the design envelope was not defined as the configuration producing the highest $NH_3$ concentration in the cavity, but as the physically feasible region where $NH_3$ transfer remained favorable while wetting safety, membrane thickness, and future sensor-placement requirements were simultaneously maintained. Thus, parameters that improved transfer were not automatically considered optimal if they introduced other limitations, such as reduced liquid-entry pressure, insufficient structural thickness, or dilution of $NH_3$ concentration in a larger cavity.

The study should be interpreted as a design-level simulation framework. The membrane was modeled as an effective porous medium, and the structural criterion was used only as a first-order lower-bound feasibility check under external pressure. Microscopic pore reconstruction, experimental sensor calibration, and long-term durability evaluation, including creep, fatigue, and aging, were beyond the present scope and are reserved for future prototype validation.

## 5. Results and Discussion

### 5.1. $NH_3$ Transfer Model and Baseline Response

The simulation results were interpreted using the $NH_3$-transfer framework introduced in Fig. 1. In this framework, the water-side ammonia condition was not represented as a generic gas concentration. Instead, the free $NH_3$ concentration available for membrane transfer was estimated from the water-side ammonium concentration, pH, and temperature based on the $NH_4^+ / NH_3$ equilibrium. Therefore, the simulated transfer process represents the movement of neutral $NH_3$ from the water domain through the spherical PTFE membrane and its accumulation in the inner cavity, which is intended for future $NH_3$ gas sensor placement.

The COMSOL geometry and domain configuration are shown in Fig. 3. The model consists of three main domains: the surrounding water domain, the porous PTFE membrane domain, and the inner cavity. In the mid-plane slice, the reddish region represents the surrounding water domain, the thin colored ring around the cavity represents the PTFE membrane layer where the concentration gradient across the membrane is visualized, and the blue circular region represents the inner cavity. The water domain provides the $NH_3$ source concentration estimated from the ammonium/free-ammonia equilibrium, while the inner cavity represents the sensor-side gas accumulation region. This modeling structure supports the design-level assumption that the membrane is not intended to transport $NH_4^+$ ions directly, but instead allows the transfer of neutral $NH_3$ through an effective porous PTFE domain.

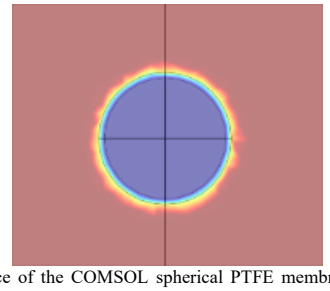


**Fig. 3.** Mid-plane slice of the COMSOL spherical PTFE membrane model, where the reddish region represents the surrounding water domain, the thin colored ring represents the PTFE membrane transfer layer, and the blue region represents the inner cavity.

Under the baseline condition, the water-side ammonium concentration was set to 1 mol/m³, with pH 8.5 and temperature 298.15 K. These values produced an estimated free $NH_3$ concentration of $1.7932 \times 10^{-1}$ mol/m³ at the water side. The simulated average $NH_3$ concentration in the inner cavity increased gradually with time and reached $6.2425 \times 10^{-4}$ mol/m³ at 100 s. The baseline parameters and response are summarized in Table 3.

**Table 3**
Baseline $NH_3$ Transfer Response.

| Parameter | Symbol | Baseline value | Role in the model |
|---|---|---|---|
| Membrane thickness | $t_{mem}$ | 1.0 mm | Diffusion path length |
| Inner radius | $r_{in}$ | 9 mm | Inner cavity size |
| Inner diameter | $D_i$ | 18 mm | Sensor cavity dimension |
| Pore size | $d_p$ | 22 µm | Transfer opening and liquid-entry pressure |
| Active pore-area fraction | $f_{active}$ | 1.0 | Effective active membrane area |
| Placement depth | $z$ | 0.3 m | Hydrostatic pressure |
| pH | pH | 8.5 | $NH_4^+ / NH_3$ equilibrium |
| Temperature | $T$ | 298.15 K | $pK_a$ and $NH_3$ availability |
| Ammonium concentration | $C_{NH4,water}$ | 1 mol/m³ | Water-side ammonia source |
| Estimated free $NH_3$ | $C_{NH_3,water}$ | $1.7932\times10^{-1}$ mol/m³ | Transferable $NH_3$ source |
| Cavity $NH_3$ at 100 s | $\overline{C}_{cavity,100s}$ | $6.2425\times10^{-4}$ mol/m³ | Sensor-side $NH_3$ response |

The time evolution of the average $NH_3$ concentration in the inner cavity is shown in Fig. 4. The cavity concentration increased continuously during the 100 s observation period, indicating that $NH_3$ accumulation in the cavity was governed by a concentration-driven transfer process from the water side through the porous PTFE membrane.

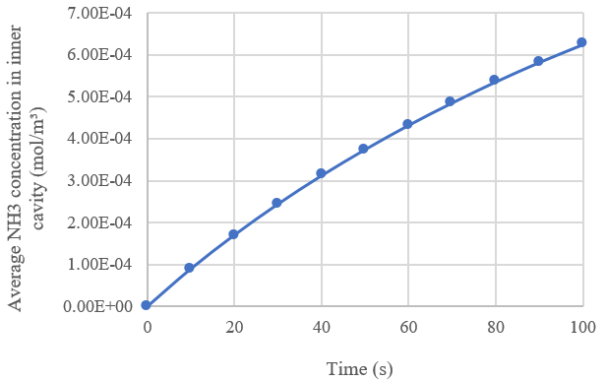



**Fig. 4.** Time evolution of the average $NH_3$ concentration in the inner cavity under the baseline condition.

At 100 s, the average cavity concentration corresponded to approximately 0.348% of the estimated water-side free $NH_3$ concentration. This indicates that the system remained in an early accumulation regime under the selected observation time. The cavity concentration was still much lower than the water-side source concentration because the PTFE membrane and inner cavity volume imposed mass-transfer resistance between the source domain and the sensor-side region.

In addition to transfer response, the baseline condition was evaluated using feasibility indicators. The hydrostatic pressure at 0.3 m depth was 2943 Pa, while the calculated liquid-entry pressure of the PTFE membrane with 22 µm pore size was 4477.4 Pa. This produced a wetting-safety factor of 1.5214, slightly above the conservative threshold of 1.5. The first-order structural check produced a critical shell pressure of $7.2047 \times 10^6$ Pa and a structural safety factor of 2367.6. The estimated minimum structural thickness was $2.517 \times 10^{-5}$ m, or approximately 25.17 µm.

**Table 4**
Baseline Feasibility Indicators

| Indicator | Symbol | Value | Interpretation |
|---|---|---|---|
| Hydrostatic pressure | $P_{hydro}$ | 2943 Pa | External water pressure at 0.3 m depth |
| Liquid-entry pressure | $LEP_{PTFE}$ | 4477.4 Pa | Estimated resistance to water intrusion |
| Wetting-safety factor | $SF_{wetting}$ | 1.5214 | Slightly above conservative threshold |
| Critical shell pressure | $P_{cr}$ | $7.2047 \times 10^6$ Pa | First-order shell feasibility |
| Structural safety factor | $SF_{struct}$ | 2367.6 | Far above lower-bound threshold |
| Minimum structural thickness | $t_{mem,min}$ | 25.17 µm | Theoretical lower-bound thickness |

These results indicate that the baseline configuration is suitable as a reference condition for subsequent parametric analysis. However, the baseline should not be interpreted as the final optimized design. The 22 µm pore size provides favorable $NH_3$ transfer, but its wetting-safety factor at 0.3 m depth is only slightly above the conservative threshold. Similarly, although the theoretical structural lower-bound thickness is much smaller than the modeled 1.0 mm membrane thickness, the final thickness interpretation must also consider material availability, fabrication robustness, and practical prototype durability. Therefore, the baseline result is used as a controlled reference for evaluating geometrical effects, water-side ammonia conditions, wetting safety, and the final design envelope in the following sections.

### 5.2. Geometrical Effects

The geometrical analysis examined how the spherical PTFE membrane structure affects $NH_3$ transfer into the inner cavity. The evaluated parameters were membrane thickness, inner diameter, pore size, and active pore-area

fraction, representing diffusion path length, cavity volume, effective transfer opening, liquid-entry resistance, and active membrane area.

Fig. 5 shows the simulated $NH_3$ total-flux streamlines at 100 s. The streamline pattern illustrates the transfer pathway from the water domain through the spherical PTFE membrane into the inner cavity. This spatial visualization supports the interpretation that $NH_3$ transfer is governed by the concentration gradient across the membrane, rather than by direct transport of $NH_4^+$ ions.

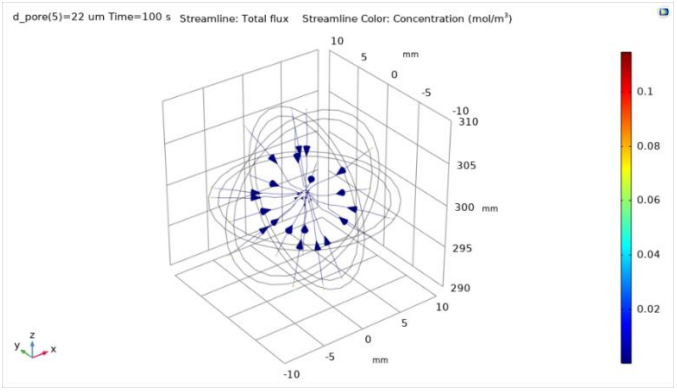



**Fig. 5.** $NH_3$ total-flux streamlines through the spherical PTFE membrane at 100 s.

The geometrical effects are summarized in Table 5. Rather than interpreting each parameter as an independent optimization target, the results are interpreted as physical tendencies that support the construction of the final design envelope.

The membrane-thickness results show that thinner membranes increased $NH_3$ transfer by shortening the diffusion pathway. At 100 s, the average cavity concentration decreased from $1.2936 \times 10^{-3}$ mol/m³ at 0.5 mm to $6.2425 \times 10^{-4}$ mol/m³ at 1.0 mm and $4.8804 \times 10^{-4}$ mol/m³ at 1.5 mm. However, the thinnest membrane should not automatically be selected because final thickness must also consider structural feasibility, fabrication robustness, material durability, and prototype reliability.

The inner-diameter results show that larger cavities reduced the average $NH_3$ concentration at 100 s. The concentration decreased from $8.1505 \times 10^{-4}$ mol/m³ at 14 mm to $6.2425 \times 10^{-4}$ mol/m³ at 18 mm and $4.9060 \times 10^{-4}$ mol/m³ at 22 mm. Thus, inner diameter represents a trade-off between sensor-placement space and sensor-side concentration response.

Pore size showed the opposite tendency. Increasing pore size from 0.5 µm to 22 µm increased the average cavity $NH_3$ concentration from $2.8295 \times 10^{-4}$ mol/m³ to $6.2425 \times 10^{-4}$ mol/m³ at 100 s, indicating that larger pores improve the effective transfer opening. However, because larger pores reduce liquid-entry pressure, pore size must be evaluated together with wetting safety. This interpretation is consistent with membrane studies showing that liquid-entry pressure and wetting resistance are strongly affected by pore structure and surface properties [15,16]. The corresponding liquid-entry pressure and wetting-safety factor at 0.3 m depth are summarized in Table 6.

The interpretation of active pore-area effects is linked to the effective porous-medium formulation and the pore-opening factor defined in equation (11). The simplified scaling is used as a dimensionless pore-opening correction factor based on the ideal assumption that the representative pore opening can be approximated as a circular area. Since the area of an ideal circular pore is proportional to the square of its diameter, the normalized opening factor scales with the square of the pore-diameter ratio. This formulation provides a consistent design-level basis for comparing the combined effects of pore size and active pore-area fraction within the proposed membrane model.

**Table 6**
Pore-Related Wetting-Safety Constraint at 0.3 m Depth.

| Pore size | $P_{hydro}$ | $LEP_{PTFE}$ | $SF_{wetting}$ | Wetting interpretation |
|---|---|---|---|---|
| 0.5 µm | 2943 Pa | $1.9700 \times 10^5$ Pa | 66.940 | Very safe |
| 1 µm | 2943 Pa | 98502 Pa | 33.470 | Very safe |
| 5 µm | 2943 Pa | 19700 Pa | 6.6940 | Safe |
| 10 µm | 2943 Pa | 9850.2 Pa | 3.3470 | Safe |
| 22 µm | 2943 Pa | 4477.4 Pa | 1.5214 | Near conservative threshold |

Table 6 shows that increasing pore size strongly reduced the liquid-entry pressure and wetting-safety factor. Although the 22 µm pore size produced the highest $NH_3$ transfer response, its wetting-safety factor was only 1.5214, which is slightly above the conservative threshold of 1.5. In contrast, smaller pores provided substantially higher wetting resistance but produced lower $NH_3$ transfer. This confirms that pore size must be interpreted as a trade-off between transfer response and wetting safety.

The active pore-area fraction also influenced the transfer response. Increasing $f_{active}$ increased the average cavity concentration from $4.2298 \times 10^{-4}$ mol/m³ at $f_{active} = 0.50$ to $4.9974 \times 10^{-4}$ mol/m³ at $f_{active} = 0.75$ and $6.2425 \times 10^{-4}$ mol/m³ at $f_{active} = 1.00$. This confirms that a larger active membrane area contributes to stronger $NH_3$ transfer. However, the maximum active area should not automatically be interpreted as the optimal design because a larger active region also increases the membrane area exposed to water. Therefore, the final interpretation must consider both transfer benefit and potential wetting exposure.

Overall, the geometrical results show that membrane geometry affects $NH_3$ transfer through different but interconnected mechanisms. Thin membranes, larger pores, and larger active pore-area fractions tend to improve transfer response, while a larger cavity size can reduce the average cavity concentration at a fixed observation time. However, the geometrically favorable trend is not automatically the final design direction. The final membrane design must be selected within a design envelope that combines transfer response, structural feasibility, liquid-entry resistance, wetting-safety factor, fabrication robustness, and material durability under water immersion.

**Table 5**
Geometrical Effects on $NH_3$ Transfer.

| Geometrical factor | Values tested | Fixed conditions | Main output at 100 s | Physical interpretation | Design implication |
|---|---|---|---|---|---|
| Membrane thickness | 0.5, 1.0, 1.5 mm | $r_{in} = 9$ mm, $d_p = 22$ µm, $f_{active} = 1$ | $1.2936 \times 10^{-3}$; $6.2425 \times 10^{-4}$; $4.8804 \times 10^{-4}$ mol/m³ | A thicker membrane increases diffusion path length and transfer resistance | Do not select the thinnest membrane solely based on transfer response |
| Inner diameter | 14, 18, 22 mm | $t_{mem} = 1$ mm, $d_p = 22$ µm, $f_{active} = 1$ | $8.1505 \times 10^{-4}$; $6.2425 \times 10^{-4}$; $4.9060 \times 10^{-4}$ mol/m³ | A larger cavity volume reduces average $NH_3$ concentration at the same observation time | Select cavity size based on sensor-placement space and response intensity |
| Pore size | 0.5, 1, 5, 10, 22 µm | $t_{mem} = 1$ mm, $r_{in} = 9$ mm, $f_{active} = 1$ | $2.8295 \times 10^{-4}$; $2.8395 \times 10^{-4}$; $3.1567 \times 10^{-4}$; $3.8167 \times 10^{-4}$; $6.2425 \times 10^{-4}$ mol/m³ | A larger pore size increases the effective transfer opening | Must be limited by liquid-entry pressure, wetting-safety factor, and material robustness |
| Active pore-area fraction | 0.50, 0.75, 1.00 | $t_{mem} = 1$ mm, $r_{in} = 9$ mm, $d_p = 22$ µm | $4.2298 \times 10^{-4}$; $4.9974 \times 10^{-4}$; $6.2425 \times 10^{-4}$ mol/m³ | A larger active area increases the membrane area contributing to $NH_3$ transfer | Maximum active area is not automatically optimal because exposed wetting area also increases |

### 5.3. Water-Side Ammonia Conditions and Wetting Safety

The water-side condition analysis was conducted to evaluate how ammonium concentration, pH, temperature, and placement depth affect $NH_3$ availability, transfer response, and wetting safety. These variables are essential because the PTFE membrane does not transport $NH_4^+$ directly. Instead, $C_{NH_4,water}$, pH, and temperature determine the amount of free $NH_3$ available for membrane transfer through the $NH_4^+/NH_3$ equilibrium. The water-side free $NH_3$ source was calculated using the equilibrium relation defined in equation (5) and the temperature-dependent $pK_a$ was calculated using equation (6).

Thus, pH and temperature determine the fraction of ammonia available as neutral $NH_3$, while $C_{NH_4,water}$ acts as the source-strength parameter. The resulting free $NH_3$ concentration then drives membrane transfer through the concentration gradient across the PTFE layer.

The pH sweep showed the strongest chemical effect. Increasing pH shifted the $NH_4^+/NH_3$ equilibrium toward neutral $NH_3$, thereby increasing the free $NH_3$ concentration at the water side. As pH increased from 6.5 to 9.0, $C_{NH_3,water}$ increased from $1.7932 \times 10^{-3}$ to $5.6705 \times 10^{-1}$ mol/m³, while the average cavity $NH_3$ concentration at 100 s increased from $6.2459 \times 10^{-6}$ to $1.9741 \times 10^{-3}$ mol/m³. This approximately 316-fold increase confirms that pH is a dominant water-side variable for membrane-assisted $NH_3$ transfer.

Temperature also influenced the cavity response through the temperature-dependent $pK_a$. As temperature increased from 293.15 K to 308.15 K, $pK_a$ decreased from 9.4025 to 8.9492, increasing $C_{NH_3,water}$ from 0.12516 to 0.35543 mol/m³. Consequently, the average cavity $NH_3$ concentration at 100 s increased from $4.3570 \times 10^{-4}$ to $1.2374 \times 10^{-3}$ mol/m³. This confirms that temperature acts as a chemical-equilibrium modifier rather than a geometrical parameter.

Under fixed pH and temperature, ammonium concentration showed an approximately proportional effect. Increasing $C_{NH_4,water}$ from 0.1 to 5.0 mol/m³ increased $C_{NH_3,water}$ from $1.7932 \times 10^{-2}$ to $8.9659 \times 10^{-1}$ mol/m³, while the average cavity $NH_3$ concentration increased from $6.2458 \times 10^{-5}$ to $3.1213 \times 10^{-3}$ mol/m³. The main water-side response results are summarized in Table 7.

Placement depth was then evaluated as a physical wetting constraint. In the present diffusion model, depth did not substantially change the cavity $NH_3$ concentration because the water-side $NH_3$ source was governed by $C_{NH_4,water}$, pH, and temperature. However, depth strongly affected wetting safety through the hydrostatic-pressure relation, the PTFE liquid-entry pressure, and the wetting-safety factor defined previously in equations (12)–(14), respectively.

The hydrophobic property of PTFE is represented in this formulation through the contact-angle term. Recent studies on gas/liquid separation membranes and membrane systems show that liquid-entry pressure, wetting resistance, surface chemistry, contact angle, and pore-size-related behavior are important indicators of membrane feasibility under liquid exposure [15,16]. In practical membrane selection, manufacturer specifications also commonly report resistance to liquid penetration using water-entry pressure, water-breakthrough pressure, or bubble-point values [22,23]. These technical indicators confirm that wetting resistance is a practical membrane property and is strongly linked to pore size and membrane construction, not merely to the polymer name PTFE alone.

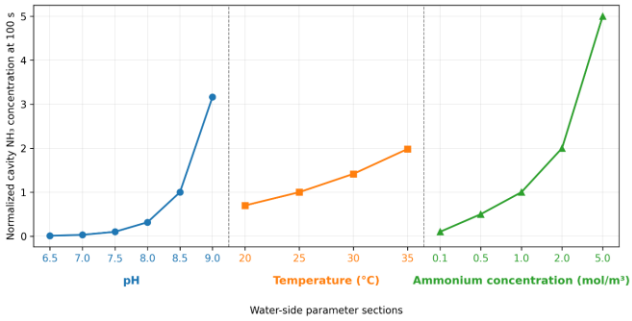



**Fig. 6.** Combined effects of pH, temperature, and ammonium concentration on the normalized average $NH_3$ concentration in the inner cavity at 100 s.

This interpretation supports the simulated wetting-safety results. Smaller-pore PTFE membranes generally provide higher resistance to liquid penetration, while larger-pore membranes provide lower resistance. This trend is consistent with the present model, where $LEP_{PTFE}$ is inversely proportional to pore diameter. Under the baseline pore size of 22 µm, $LEP_{PTFE}$ was 4477.4 Pa. As placement depth increased from 0.1 m to 0.55 m, $P_{hydro}$ increased from 981.0 Pa to 5395.5 Pa, reducing $SF_{wetting}$ from 4.5641 to 0.8298. The wetting-safety response is summarized in Table 8.

**Table 7**
Water-Side $NH_3$ Availability and Transfer Response.

| Water-side factor | Values tested | Fixed conditions | $C_{NH_3,water}$ | Cavity $NH_3$ at 100 s | Physical interpretation |
|---|---|---|---|---|---|
| pH | 6.5 | $C_{NH_4}=1$, $T=298.15$ K, $z=0.3$ m | $1.7932 \times 10^{-3}$ | $6.2459 \times 10^{-6}$ | Low free $NH_3$ availability |
| pH | 7.0 | same | $5.6705 \times 10^{-3}$ | $1.9753 \times 10^{-5}$ | $NH_3$ still limited |
| pH | 7.5 | same | $1.7932 \times 10^{-2}$ | $6.2458 \times 10^{-5}$ | $NH_3$ begins to increase |
| pH | 8.0 | same | $5.6705 \times 10^{-2}$ | $1.9741 \times 10^{-4}$ | Higher free $NH_3$ fraction |
| pH | 8.5 | same | $1.7932 \times 10^{-1}$ | $6.2425 \times 10^{-4}$ | Baseline response |
| pH | 9.0 | same | $5.6705 \times 10^{-1}$ | $1.9741 \times 10^{-3}$ | Strong $NH_3$ availability |
| Temperature | 20°C | pH = 8.5, $C_{NH_4}=1$, $z=0.3$ m | 0.12516 | $4.3570 \times 10^{-4}$ | Lower $NH_3$ availability |
| Temperature | 25°C | same | 0.17932 | $6.2425 \times 10^{-4}$ | Baseline |
| Temperature | 30°C | same | 0.25389 | $8.8385 \times 10^{-4}$ | Increased $NH_3$ availability |
| Temperature | 35°C | same | 0.35543 | $1.2374 \times 10^{-3}$ | Stronger $NH_3$ response |
| $C_{NH_4,water}$ | 0.1 mol/m³ | pH = 8.5, $T=298.15$ K, $z=0.3$ m | $1.7932 \times 10^{-2}$ | $6.2458 \times 10^{-5}$ | Low source strength |
| $C_{NH_4,water}$ | 0.5 mol/m³ | same | $8.9659 \times 10^{-2}$ | $3.1213 \times 10^{-4}$ | Proportional increase |
| $C_{NH_4,water}$ | 1.0 mol/m³ | same | $1.7932 \times 10^{-1}$ | $6.2425 \times 10^{-4}$ | Baseline |
| $C_{NH_4,water}$ | 2.0 mol/m³ | same | $3.5864 \times 10^{-1}$ | $1.2485 \times 10^{-3}$ | Proportional increase |
| $C_{NH_4,water}$ | 5.0 mol/m³ | same | $8.9659 \times 10^{-1}$ | $3.1213 \times 10^{-3}$ | High source strength |

**Table 8**
Wetting-Safety Constraint under Placement Depth for $d_p$ = 22 µm.

| Pore size | Depth | $P_{hydro}$ | $LEP_{PTFE}$ | $SF_{wetting}$ | Cavity $NH_3$ at 100 s | Design status |
|---|---|---|---|---|---|---|
| 22 µm | 0.10 m | 981.0 Pa | 4477.4 Pa | 4.5641 | $6.2311 \times 10^{-4}$ | Safe |
| 22 µm | 0.30 m | 2943.0 Pa | 4477.4 Pa | 1.5214 | $6.2425 \times 10^{-4}$ | Near conservative threshold |
| 22 µm | 0.50 m | 4905.0 Pa | 4477.4 Pa | 0.9128 | $6.1581 \times 10^{-4}$ | Wetting risk |
| 22 µm | 0.55 m | 5395.5 Pa | 4477.4 Pa | 0.8298 | $6.1671 \times 10^{-4}$ | Wetting risk |

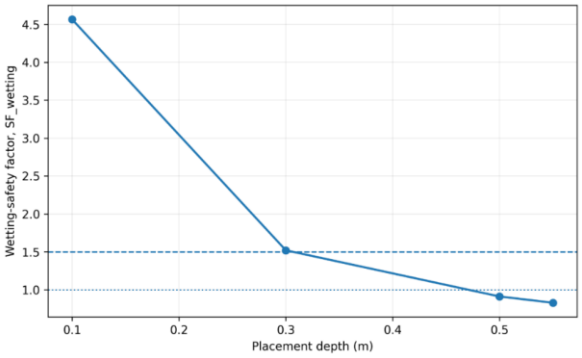



**Fig. 7.** Effect of placement depth on wetting-safety factor for the 22 µm pore-size configuration.

For $d_p = 22$ µm, the wetting-safety factor decreased from 4.5641 at 0.1 m to 1.5214 at 0.3 m, then dropped below unity at 0.5 m and 0.55 m. This indicates that the 22 µm pore size may provide favorable $NH_3$ transfer, but it becomes depth-limited. At 0.3 m, it remains only slightly above the conservative threshold of $SF_{wetting} \geq 1.5$. At 0.5 m and deeper within the valid tank geometry, the configuration becomes wetting-risk under the present assumptions.

Therefore, the water-side and wetting analyses show two complementary constraints. The chemical source condition is governed by pH, temperature and $C_{NH_4,water}$ through the $NH_4^+ / NH_3$ equilibrium, whereas placement depth controls physical feasibility through hydrostatic pressure and wetting safety. When combined with industrial PTFE membrane datasheet evidence, the results indicate that a large pore size such as 22 µm should be interpreted as transfer-favorable but wetting-limited [15,16]. More conservative pore sizes may reduce $NH_3$ transfer but provide a stronger wetting-resistance margin for future gas-sensor integration in water.

### *5.4. Integrated Design Envelope for Future* $NH_3$ *Gas-Sensor Integration*

The integrated design-envelope analysis combines the geometrical results, water-side ammonia response, wetting-safety constraint, and future gas sensor integration requirement. The purpose is not to select the configuration that produces the maximum $NH_3$ concentration, but to identify a physically feasible and sensor-compatible PTFE membrane design for future $NH_3$ gas sensor integration in water.

The design-envelope interpretation was developed from three main considerations. First, the membrane must provide sufficient $NH_3$ transfer into the inner cavity. Second, the membrane must maintain adequate wetting resistance under hydrostatic pressure. Third, the cavity must be compatible with future $NH_3$ gas sensor placement. Recent $NH_3$ gas sensor studies have demonstrated ppm to sub-ppm detection capability at room temperature, including material-based and electrochemical $NH_3$ sensing approaches [20,21]. In addition, commercially available electrochemical or solid-polymer $NH_3$ sensors with 0–100 ppm measurement ranges include SGX/Amphenol PS1-NH3-100, Membrapor NH3/MR-100, and Winsen ME3-NH3 [24–26]. These sensor specifications support the practical relevance of providing an internal cavity for future low-level $NH_3$ gas sensing.

The simulated $NH_3$ accumulation in the inner cavity should be interpreted as a membrane-side exposure indicator, not as the complete response time of a future sensor device. In practice, electrochemical sensor response time will also depend on sensor sensitivity, cavity volume, gas mixing, diffusion-barrier characteristics, and detection threshold. Therefore, full response-time validation remains necessary in future prototype testing.

The inner cavity size was therefore interpreted from a sensor-integration perspective. Although smaller cavities produced higher average $NH_3$ concentrations, an overly small cavity may limit future sensor placement, internal gas accumulation, and housing tolerance. Commercial $NH_3$ sensor specifications also indicate that several candidate sensors are within the compact electrochemical gas-sensor size class, supporting the selection of a cavity that is not only concentration-responsive but also physically compatible with future sensor integration [24–26]. Therefore, the 22 mm inner diameter was selected as a practical compromise between sensor-side concentration response and future sensor-integration space.

The active pore-area fraction was also selected based on practical membrane interpretation rather than maximum idealized exposure. In practical membrane selection, PTFE membrane specifications may report porosity, pore size, water-entry pressure, and bubble-point values as technical indicators for prototype screening [22,23]. Therefore, $f_{active} = 0.75$ was used as a representative intermediate active-area fraction for the final design, rather than assuming full active exposure over the entire membrane surface. This value represents a practical design compromise because a larger active area may increase $NH_3$ transfer, but it also increases the membrane area exposed to water and may increase potential wetting exposure.

Fig. 8 shows the final design-envelope map based on pore size and placement depth. The conservative wetting-safety threshold $SF_{wetting} = 1.5$ separates the recommended wetting-safe region from configurations close to or below the wetting-safety limit. The previous transfer-favorable 22 µm design at 0.3 m is located close to this threshold, while the final recommended 10 µm design at 0.3 m provides a wider wetting-safety margin.

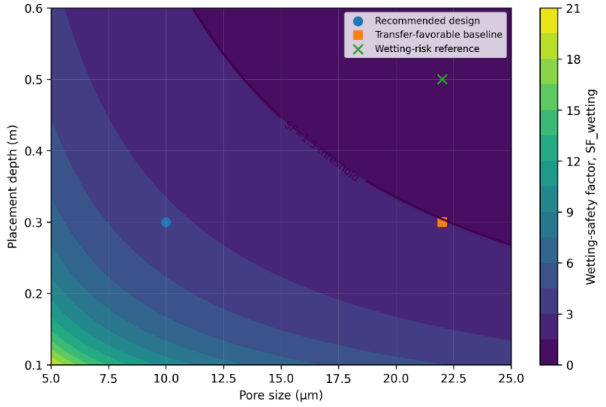



**Fig. 8.** Integrated design-envelope map showing the relationship between pore size, placement depth, and wetting-safety factor for spherical PTFE membrane selection.

**Table 9**
Integrated Design-Envelope Logic.

| Design factor | Physical / chemical basis | Response tendency | Limiting constraint | Design-envelope implication |
|---|---|---|---|---|
| Membrane thickness | Fickian diffusion | Thinner membrane increases $NH_3$ transfer | Structural feasibility and prototype robustness | 1.0 mm selected as a balanced thickness |
| Inner diameter | Cavity accumulation geometry | Smaller cavity increases average concentration | Sensor placement and housing tolerance | 22 mm selected for sensor compatibility |
| Pore size | Effective opening and Young–Laplace liquid-entry pressure | Larger pore increases transfer | Larger pore lowers $LEP_{PTFE}$ and $SF_{wetting}$ | 10 µm selected for stronger wetting margin |
| Active pore-area fraction | Effective active porosity | Larger active area increases transfer | Larger exposed active area may increase wetting exposure | 0.75 selected as representative intermediate active area |
| pH | $NH_4^+ / NH_3$ equilibrium | Higher pH increases free $NH_3$ | Real water chemistry | Must be considered in sensor-response interpretation |
| Temperature | Temperature-dependent $pK_a$ | Higher temperature increases free $NH_3$ availability | Operating condition | Temperature correction is required |
| $NH_4^+$ concentration | Source-strength relation | Higher $C_{NH_4,water}$ increases free $NH_3$ source | Real water condition and sensor range | $NH_4^+$ is the source condition, not the transported species |
| Placement depth | Hydrostatic pressure | Does not substantially change $NH_3$ source | Higher depth reduces $SF_{wetting}$ | Safe depth depends strongly on pore size |

Before constructing the pore-size and active pore-area trade-off summary, two design variables were first constrained based on the preceding geometrical analysis. The membrane thickness was retained at 1.0 mm because Table 5 shows that thinner membranes increase cavity ammonia accumulation, whereas thickness also contributes to structural feasibility through the thin spherical shell relation in equation (16) and the structural safety factor in equation (18). The inner diameter was fixed at 22 mm based on the inner-diameter trend in Table 5, where a larger cavity reduces average concentration but provides the practical cavity space required for future gas-sensor placement. Accordingly, the subsequent trade-off matrix focuses on pore size and active pore-area fraction.

Based on this trade-off summary, the recommended configuration was validated using 1.0 mm membrane thickness, 22 mm inner diameter, 10 μm pore size, and 0.75 active pore-area fraction at 0.3 m placement depth. The final validation results are summarized in Table 11.

The final recommended design produced a lower cavity $NH_3$ concentration than the earlier transfer-favorable 22 μm configuration. However, this reduction was intentional. The 22 μm configuration produced higher transfer but had $SF_{wetting} = 1.5214$ at 0.3 m, only slightly above the conservative threshold. In contrast, the 10 μm final design produced $\overline{C}_{cavity,100s} = 2.7049 \times 10^{-4}$ mol/m³ while maintaining $SF_{wetting} = 3.3470$. This indicates a more robust design against unintended deeper placement and wetting risk.

Fig. 9 presents the COMSOL multi-slice visualization of the final recommended design configuration using $t_{mem} = 1.0$ mm, $D_i = 22$ mm, $d_p = 10$ μm, $f_{active} = 0.75$, and $z_{depth} = 0.3$ m. The visualization shows the spherical PTFE membrane position within the water domain and the enlarged inner cavity intended for future $NH_3$ gas sensor integration. This figure supports the final design-envelope interpretation by showing the sensor-compatible membrane configuration after combining transfer response, wetting safety, structural feasibility, and sensor accommodation constraints.

The combined interpretation shows that the final design should not be selected from maximum $NH_3$ transfer alone. Instead, membrane geometry, water-side $NH_3$ availability, wetting safety, structural feasibility, and sensor compatibility must be considered together. Thus, the suitable configuration is a balanced design region that preserves measurable $NH_3$ transfer while maintaining wetting resistance and practical feasibility for future gas sensor integration.

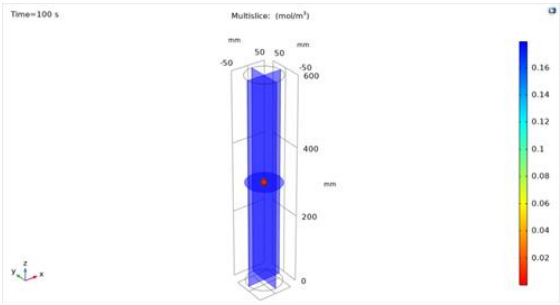



**Fig. 9**. COMSOL multi-slice visualization of the final recommended spherical PTFE membrane design for future $NH_3$ gas sensor integration.

### 5.5. Additional Physical Effects for Future Model Refinement

As an additional sensitivity consideration, the concentration-based equilibrium relation used to define the water-side $NH_3$ source was evaluated against possible activity-coefficient effects. The present study is intended for controlled freshwater aquaculture conditions rather than brackish, saline, or industrial wastewater matrices. Nevertheless, ionic strength has been reported to affect ammonia ionization and unionized ammonia estimation [27], while ammonia/ammonium dissociation is also influenced by temperature, pH, and ionic strength or salinity [28]. For this screening estimate, $NH_3$ was treated as a neutral species with $\gamma_{NH_3} \approx 1$, while $\gamma_{NH_4^+}$ was estimated using a Davies-type activity-coefficient relation [29]. The relative overestimation of free $NH_3$ caused by neglecting $\gamma_{NH_4^+}$ was calculated as $\left(1/\gamma_{NH_4^+} - 1\right) \times 100\%$, as summarized in Table 12.

**Table 10**
Compact trade-off matrix for pore size and active pore-area selection.

| Configuration | Main quantitative result | Trade-off interpretation + case | Manuscript basis |
|---|---|---|---|
| $d_p = 22\,\mu m$; $f_{active} = 1.00$ | Cavity $NH_3$ = 6.2425 × 10⁻⁴ mol/m³; $SF_{wetting}$ = 1.5214; $SF_{struct}$ = 2367.6 | Baseline transfer-favorable case. Highest reported baseline $NH_3$ response, but the wetting margin is very close to the conservative threshold. | Baseline response and feasibility indicators; Tables 4–5; pore-related wetting constraint in Table 6 |
| $d_p = 22\,\mu m$; $f_{active} = 0.75$ | Not directly simulated as a combined case; $SF_{wetting}$ remains governed by $d_p$ = 22 μm, i.e., 1.5214 | Reduced-active but wetting-limited case. Lower active exposure may reduce the active transfer region, but it does not address the pore-controlled wetting limitation. | Inferred from active-area trend in Table 5 and pore-related wetting constraint in Table 6 |
| $d_p = 10\,\mu m$; $f_{active} = 1.00$ | Cavity $NH_3$ lower than the 22 μm baseline case; $SF_{wetting}$ = 3.3470 | Wetting-safer full-active case. Smaller pore size improves wetting safety, but full active exposure remains less conservative than the selected intermediate active area. | Pore-size sweep in Table 5 and wetting constraint in Table 6 |
| $d_p = 10\,\mu m$; $f_{active} = 0.75$ | Cavity $NH_3$ = 2.7049 × 10⁻⁴ mol/m³; $SF_{wetting}$ = 3.3470; $SF_{struct}$ = 1615.7 | Final balanced design. Combines stronger wetting safety, intermediate active exposure, structural feasibility, and sensor-compatible cavity sizing. | Final validation simulation; Table 11 |

**Table 11**
Final Recommended Design Configuration and Validation Result.

| Parameter / indicator | Final value | Design interpretation |
|---|---|---|
| Membrane thickness, $t_{mem}$ | 1.0 mm | Balanced transfer and robustness |
| Inner diameter, $D_i$ | 22 mm | Practical cavity size for future $NH_3$ gas sensor integration |
| Pore size, $d_p$ | 10 μm | Improved wetting margin compared with 22 μm |
| Active pore-area fraction, $f_{active}$ | 0.75 | Representative intermediate active-area fraction |
| Placement depth, $z_{depth}$ | 0.3 m | Shallow-water operating condition |
| $C_{NH_3,water}$ | 0.17932 mol/m³ | Baseline free $NH_3$ source |
| $\overline{C}_{cavity,100s}$ | 2.7049 × 10⁻⁴ mol/m³ | Final sensor-side $NH_3$ response |
| $LEP_{PTFE}$ | 9850.2 Pa | Liquid-entry resistance for 10 μm pore size |
| $SF_{wetting}$ | 3.3470 | Above conservative threshold of 1.5 |
| $SF_{struct}$ | 1615.7 | Structurally feasible |
| $D_{mem,eff}$ | 5.4236 × 10⁻¹¹ m²/s | Effective diffusivity under final active-area setting |

**Table 12**
Screening-level activity-coefficient sensitivity estimate for free $NH_3$ calculation.

| Ionic-strength condition | Interpretation in this study | Estimated $\gamma_{NH_4^+}$ | Estimated overestimation of free $NH_3$ if activity is ignored |
|---|---|---|---|
| $I = 0.001$ M | Controlled dilute freshwater aquaculture condition | 0.965 | 3.6% |
| $I = 0.010$ M | Upper freshwater-like sensitivity boundary | 0.902 | 10.9% |

The estimate shows that the activity-coefficient effect is limited under the controlled dilute freshwater condition targeted in this study, with approximately 3.6% overestimation. Therefore, the concentration-based Henderson–Hasselbalch formulation remains appropriate for the present design-level COMSOL framework. However, the upper sensitivity boundary indicates that the error becomes non-negligible as ionic strength increases; therefore, activity-based speciation correction should be included in future applications involving brackish, saline, or chemically complex waters.

Beyond activity correction, several physical effects were not explicitly resolved in the present design-level simulation. The pore-opening factor was treated as an effective area-based correction; therefore, pore-size distribution, pore interconnectivity, and anisotropic pore morphology may influence the actual effective diffusivity of a fabricated membrane. Similarly, the wetting-safety criterion was based on static LEP estimation, whereas transient pressure variations, dynamic wetting, and local defects may affect practical wetting reliability. The structural feasibility analysis also used pristine PTFE properties and first-order shell theory; therefore, porosity-dependent modulus reduction and viscoelastic creep may influence long-term shell stability. Finally, the COMSOL model was formulated as a purely diffusive transport model with flux continuity across domains, so concentration polarization, interfacial mass-transfer resistance, and convective effects near the membrane surface were not explicitly resolved. These aspects are appropriate to address in subsequent refinement stages through the iterative modeling–prototyping–evaluation cycle.

## 6. Conclusion

This study developed a physics-based COMSOL framework to evaluate $NH_3$ transfer through a spherical PTFE membrane immersed in water. Unlike a generic gas-transfer model, the framework explicitly considers the water-side $NH_4^+ / NH_3$ equilibrium, where $NH_4^+$ is not treated as the transported species. Instead, free $NH_3$ is estimated from the water-side $NH_4^+$ concentration, pH, and temperature, and is then modeled as the transferable species through the hydrophobic PTFE membrane into the inner cavity. This formulation provides a physically meaningful basis for future $NH_3$ gas sensor integration.

In response to RQ1, the results show that the geometrical characteristics of the spherical PTFE membrane affect $NH_3$ transfer through different physical mechanisms. Membrane thickness controls the diffusion path length, inner diameter determines the cavity size for gas accumulation and sensor accommodation, pore size affects both the effective transfer opening and liquid-entry resistance, and active pore-area fraction controls the effective membrane area available for $NH_3$ transfer. Therefore, membrane geometry should not be interpreted only from maximum transfer response, because each transfer-favorable direction must also be evaluated against structural feasibility, wetting resistance, and practical fabrication constraints.

In response to RQ2, the water-side conditions influence the system through both chemical and physical pathways. The $NH_4^+ / NH_3$ equilibrium determines the amount of free $NH_3$ available for transfer, where $pH$ and temperature control the equilibrium shift and water-side $NH_4^+$ concentration acts as the source-strength parameter. In contrast, placement depth mainly affects wetting safety by increasing hydrostatic pressure rather than directly modifying the $NH_3$ source concentration. Thus, water-side conditions must be treated not only as operating variables, but also as design constraints for membrane-assisted $NH_3$ transfer in water.

In response to RQ3, the suitable membrane configuration is best defined as a design envelope rather than a maximum-response configuration. The recommended design uses a 1.0 mm membrane thickness, 22 mm inner diameter, 10 µm pore size, and 0.75 active pore-area fraction at 0.3 m placement depth. This configuration produced an average cavity $NH_3$ concentration of $2.7049 \times 10^{-4}$ mol/m³ at 100 s, while maintaining $SF_{wetting} = 3.3470$ and $SF_{struct} = 1615.7$. The 22 mm cavity supports future low-ppm electrochemical $NH_3$ gas sensor integration, while the 10 µm pore size provides a stronger wetting-safety margin than the transfer-favorable but threshold-limited 22 µm pore configuration.

The main contribution of this study is the establishment of a physics-based design-envelope framework for a spherical PTFE membrane intended for future $NH_3$ gas sensor integration in water. The framework links membrane geometry, $NH_4^+ / NH_3$ equilibrium, Fickian transfer, hydrostatic pressure, liquid-entry constraints, and sensor-compatible cavity sizing within a single design-oriented analysis. This makes the study an early-stage engineering design foundation rather than only a numerical transfer exercise.

Since the present framework is intended for controlled freshwater design conditions, several detailed physical effects remain outside the current design-level simulation, as discussed in section 5.5. These include activity-coefficient effects under higher ionic strength, pore-morphology effects on effective diffusivity, practical wetting-reliability factors, long-term structural effects, and additional transport effects near the membrane surface. Future work is expected to extend the framework through an iterative modeling–prototyping–evaluation cycle. Experimental findings from prototype evaluation are intended to be used to refine the COMSOL model and guide subsequent membrane-design improvements.

## Authorship Contributions

Maulana Fakih Latief contributed to conceptualization, methodology, software implementation, formal analysis, investigation, visualization, and writing of the original manuscript draft. Benfano Soewito contributed to supervision, validation, technical guidance, and manuscript review and editing. Maria Susan Anggreainy contributed to conceptualization, methodology refinement, and manuscript review and editing. Suryadiputra Liawatimena contributed to methodological design, validation, supervision, and manuscript review and editing. All authors have read and approved the final version of the manuscript.

## Data Availability Statement

No external dataset was used in this study. The simulation data supporting the findings of this study are presented within the article.

## Disclosure Statement

The authors declare that they have no competing interests.

## Funding

No funding was received for this research.

## CRediT authorship contribution statement

*M. F. Latief*: Conceptualization; Methodology; Software; Formal analysis; Investigation; Visualization; Writing – original draft.
*B. Soewito*: Supervision; Validation; Methodology; Writing – review & editing.
*M. S. Anggreainy*: Conceptualization; Methodology; Writing – review & editing.
*S. Liawatimena*: Methodology; Validation; Supervision; Writing – review & editing.

## References

[1] M. Li, Z. Zhu, M. Zhou, X. Jie, L. Wang, G. Kang, and Y. Cao, "Removal of CO_2 from biogas by membrane contactor using PTFE hollow fibers with smaller diameter," Journal of Membrane Science, vol. 627, p. 119232, 2021, https://doi.org/10.1016/j.memsci.2021.119232.

[2] Q. Guo, Y. Huang, M. Xu, Q. Huang, J. Cheng, S. Yu, Y. Zhang, and C. Xiao, "PTFE porous membrane technology: A comprehensive review," Journal of Membrane Science, vol. 664, p. 121115, 2022, https://doi.org/10.1016/j.memsci.2022.121115.

[3] H. Kim, T. Yun, S. Hong, and S. Lee, "Experimental and theoretical investigation of a high performance PTFE membrane for vacuum-

membrane distillation," Journal of Membrane Science, vol. 617, p. 118524, 2021, https://doi.org/10.1016/j.memsci.2020.118524.

[4] Y. Zhu, H. Chang, Z. Yan, C. Liu, Y. Liang, F. Qu, H. Liang, and R. D. Vidic, "Review of ammonia recovery and removal from wastewater using hydrophobic membrane distillation and membrane contactor," Separation and Purification Technology, vol. 328, p. 125094, 2024, https://doi.org/10.1016/j.seppur.2023.125094.

[5] K. Yang, B. M. Simplot, and M. Qin, "Dual effect of solution pH on ammonia recovery in membrane distillation: Influence on pH partitioning and mass transfer coefficient," ACS ES&T Engineering, vol. 5, no. 11, pp. 2855–2863, 2025, https://doi.org/10.1021/acsestengg.5c00332.

[6] P. P. Kywe and C. Ratanatamskul, "Influences of permeate solution and feed pH on enhancement of ammonia recovery from wastewater by negatively charged PTFE membranes in direct contact membrane distillation operation," ACS Omega, vol. 7, no. 31, pp. 27722–27733, 2022, https://doi.org/10.1021/acsomega.2c03673.

[7] R. A. Al-Juboori, M. Al-Shaeli, S. A. Aani, D. Johnson, and N. Hilal, "Membrane technologies for nitrogen recovery from waste streams: Scientometrics and technical analysis," Membranes, vol. 13, no. 1, art. no. 15, 2023, https://doi.org/10.3390/membranes13010015.

[8] P. Woźniak and M. Gryta, "Wettability studies of capillary PTFE membranes applied for membrane distillation," Membranes, vol. 13, no. 1, art. no. 80, 2023, https://doi.org/10.3390/membranes13010080.

[9] W. Ma, R. Han, L. Zhu, L. Jiang, W. Zhang, H. Zhang, and L. Chen, "Efficient recovery of ammonia from digestate by membrane distillation: Nano-FeOOH re-entry structure modification, anti-fouling, and anti-wetting performance," Separation and Purification Technology, vol. 323, p. 124414, 2023, https://doi.org/10.1016/j.seppur.2023.124414.

[10] M. Soto-Herranz, M. Sánchez-Báscones, J. M. Antolín-Rodríguez, and P. Martín-Ramos, "Evaluation of different capture solutions for ammonia recovery in suspended gas permeable membrane systems," Membranes, vol. 12, no. 6, art. no. 572, 2022, https://doi.org/10.3390/membranes12060572.

[11] M. Soto-Herranz, M. Sánchez-Báscones, M. C. García-González, and P. Martín-Ramos, "Comparison of the ammonia trapping performance of different gas-permeable tubular membrane system configurations," Membranes, vol. 12, no. 11, art. no. 1104, 2022, https://doi.org/10.3390/membranes12111104.

[12] K. Yang and M. Qin, "Understanding ammonia and water transport in direct contact membrane distillation toward selective ammonia recovery," ACS ES&T Engineering, vol. 4, no. 6, pp. 1321–1330, 2024, https://doi.org/10.1021/acsestengg.3c00623.

[13] Y. Hu, C. Y. Loh, M. Xie, G. Chen, M. Huang, and J. Qiao, "Ammonia recovery via direct contact membrane distillation: Modeling and performance optimization," Journal of Environmental Management, vol. 365, p. 121683, 2024, https://doi.org/10.1016/j.jenvman.2024.121683.

[14] A.-C. Bozonc, V.-C. Sandu, C.-C. Cormos, and A.-M. Cormos, "3D-CFD modeling of hollow-fiber membrane contactor for CO_2 absorption using MEA solution," Membranes, vol. 14, no. 4, art. no. 86, 2024, https://doi.org/10.3390/membranes14040086.

[15] S. Claramunt, F. Völker, U. Gerhards, M. Kraut, and R. Dittmeyer, "Membranes for the gas/liquid phase separation at elevated temperatures: Characterization of the liquid entry pressure," Membranes, vol. 11, no. 12, art. no. 907, 2021, https://doi.org/10.3390/membranes11120907.

[16] A. Samadi, T. Ni, E. Fontananova, G. Tang, H. Shon, and S. Zhao, "Engineering antiwetting hydrophobic surfaces for membrane distillation: A review," Desalination, vol. 563, p. 116722, 2023, https://doi.org/10.1016/j.desal.2023.116722.

[17] Z. Xiong, Q. Lai, J. Lu, F. Qu, H. Yu, X. Chen, G. Zhang, W. Zhang, and S. Zhao, "Silanization enabled superhydrophobic PTFE membrane with antiwetting and antifouling properties for robust membrane distillation," Journal of Membrane Science, vol. 674, p. 121546, 2023, https://doi.org/10.1016/j.memsci.2023.121546.

[18] L. Francis and N. Hilal, "Electrohydrodynamic atomization of CNT on PTFE membrane for scaling resistant membranes in membrane distillation," npj Clean Water, vol. 6, art. no. 15, 2023, https://doi.org/10.1038/s41545-023-00229-x.

[19] S. K. Hong, H. Kim, H. Lee, G. Lim, and S. J. Cho, "A pore-size tunable superhydrophobic membrane for high-flux membrane distillation," Journal of Membrane Science, vol. 641, p. 119862, 2022, https://doi.org/10.1016/j.memsci.2021.119862.

[20] M. Luo, X. Huang, D. Xiong, S. Cai, S. Li, Z. Jia, and Z. Gao, "Fast response/recovery and sub-ppm ammonia gas sensors based on a novel $V_2CTx$@$MoS_2$ composite," Journal of Materials Chemistry A, vol. 12, pp. 12225–12236, 2024, https://doi.org/10.1039/D4TA00842A.

[21] L. Gong, S. Jin, R. Liu, Z. Liu, Y. Zhang, L. Zhang, T. Zhao, H. Fa, and W. Yin, "A novel electrochemical ammonia sensor based on Pt NPs@MIL101(Cr)-$NH_2$ for chemical leaks detection at room temperature," Microchemical Journal, vol. 205, p. 111262, 2024, https://doi.org/10.1016/j.microc.2024.111262.

[22] Sterlitech Corporation, "PTFE Laminated Membrane Filters," product specifications. Accessed: May 10, 2026. [Online]. Available: https://www.sterlitech.com/ptfe-laminated-membrane-filters-0-1-micron-13mm-100-pk.html

[23] Pall Corporation, "Acro® 37 TF Vent Device," product datasheet, May 2018. Accessed: May 10, 2026. [Online]. Available: https://www.pall.com/content/dam/pall/pall-corp/literature-library/non-gated/product-type/vent-filters/18-0418_Acro_37_DS.pdf

[24] SGX Sensortech, "PS1-NH3-100 Ammonia 100 ppm sensor," product datasheet. Accessed: May 10, 2026. [Online]. Available: https://sgxsensortech.com/sensor/ps1-nh3-100

[25] Membrapor AG, "Ammonia gas sensor NH3/MR-100," specification sheet, Jul. 2023. Accessed: May 10, 2026. [Online]. Available: https://www.membrapor.ch/sheet/Ammonia-Gas-Sensor-NH3-MR-100.pdf

[26] Zhengzhou Winsen Electronics Technology Co., Ltd., "ME3-NH3 gas sensor," product datasheet. Accessed: May 10, 2026. [Online]. Available: https://www.winsen-sensor.com/product/me3-nh3.html

[27] R. W. Soderberg and J. W. Meade, "The effects of ionic strength on un-ionized ammonia concentration," The Progressive Fish-Culturist, vol. 53, no. 2, pp. 118–120, 1991, https://doi.org/10.1577/1548-8640(1991)053<0118:TEOISO>2.3.CO;2.

[28] T. G. Bell, M. T. Johnson, T. D. Jickells, and P. S. Liss, "Ammonia/ammonium dissociation coefficient in seawater: A significant numerical correction," Environmental Chemistry, vol. 4, no. 3, pp. 183–186, 2007, https://doi.org/10.1071/EN07032.

[29] C. W. Davies, "The extent of dissociation of salts in water. Part VIII. An equation for the mean ionic activity coefficient of an electrolyte in water, and a revision of the dissociation constants of some sulphates," Journal of the Chemical Society, pp. 2093–2098, 1938, https://doi.org/10.1039/JR9380002093.